

Comprehensive Study of Isobutane Selective Oxidation Over Group I and II Phosphomolybdates: Structural and Kinetic Factors

Shane Kendel · Trevor Brown

Received: 4 August 2011 / Accepted: 26 September 2011 / Published online: 12 October 2011
© Springer Science+Business Media, LLC 2011

Abstract Various phosphomolybdates were synthesized using cations from Groups 1 and 2 of the periodic table. These compounds were of the form $M_xH_{3-xn}[PMo_{12}O_{40}]_n$, with n being the cationic charge (+1 or +2). XRD analysis shows pure phosphomolybdic acid has a triclinic structure. A body centered cubic (BCC) structure gradually develops with addition of Group 1 cations, and the triclinic phase is completely replaced by the BCC phase once metal cations occupy a volume greater than $9\text{--}11 \text{ \AA}^3$ per phosphomolybdate anion. The Group 2 compounds do not form a cubic phase, however the triclinic phase distorts once cationic volume is greater about 5 or 6 \AA^3 and appears to become somewhat amorphous. Isobutane selective oxidation over the compounds yielded methacrolein (primary product), 3-methyl-2-oxetanone (lactone), acetic acid, propene, methacrylic acid, carbon dioxide and water as products. Propene was formed over the Group 1 compounds exclusively and methacrylic acid formation was observed with $BaH[PMo_{12}O_{40}]$ only. Products form via two distinct processes: Category 1 product has an exponential profile and coverage is consistent with a Langmuir model, Category 2 formations are consistent with desorptions from within the bulk of the substrates. Methacrolein forms via both Category 1 and 2 processes, whilst all other products are formed by Category 2 exclusively. A rigorous kinetic analysis yielded accurate activation parameters. Category 1 methacrolein formation apparent activation energies ranged from 34.7 ± 1.3 to $119 \pm 4 \text{ kJ mol}^{-1}$. Category 2 formations ranged from 34.3 ± 0.4 to $726 \pm 172 \text{ kJ mol}^{-1}$. No relationship between activity and composition or structure

could be ascertained, despite investigation into correlations using several different models.

Keywords Kinetics · Selective oxidation · Methacrolein · Heteropoly compounds · Phosphomolybdates

1 Introduction

Heteropoly compounds are useful for a large range of reactions, including alkylations, dehydrogenations, dehydrations and selective oxidations [1]. The unique structural aspects of the substrates heavily influences their activity and selectivity. There are three structural components of heteropoly compounds [2]:

- (i) *Primary structure*: The heteropolyanion or polyoxo-anion molecule
- (ii) *Secondary structure*: The arrangement of the primary structure, together with counter cations and other molecules such as water
- (iii) *Tertiary structure*: The way in which the secondary structure assembles itself into solid particles

Understanding the difference between the primary and secondary structures is essential in order to understand the reaction processes involved with these compounds [3]. The secondary structure is usually regular, though reactant molecules are able to absorb deep into the bulk of the solid and facilitates bulk-type catalysis. As a consequence, the secondary structure is the most important aspect in determining the catalytic activity of heteropoly compounds. Heteropoly compounds have both microporous and mesoporous character, but do not exhibit extensive macroporosity. The small pores of heteropoly compounds generally result in low surface areas [4, 5]. XRD studies have

S. Kendel (✉) · T. Brown
School of Science and Technology, University of New England,
Armidale, NSW 2351, Australia
e-mail: shane.kendell@gmail.com

identified several phases, including triclinic, primitive and body-centered cubic [6–14]. The degree of hydration heavily influences unit cell dimensions, whereby complete phase changes can occur [15]. The fully substituted magnesium, calcium, strontium and barium salts ($\text{Mg}_{1.5}[\text{PMo}_{12}\text{O}_{40}]$, $\text{Ca}_{1.5}[\text{PMo}_{12}\text{O}_{40}]$, $\text{Sr}_{1.5}[\text{PMo}_{12}\text{O}_{40}]$ and $\text{Ba}_{1.5}[\text{PMo}_{12}\text{O}_{40}]$), have been prepared and analyzed by McGarvey and Moffat [16]. The publication reported that the XRD data of the divalent compounds was “largely featureless”. Silviani and Burns [12] have also investigated the diffraction spectra of the alkaline earth phosphomolybdates and observed only a cubic structure without evidence of any amorphous or other phases (including triclinic).

Heteropoly compounds such as phosphomolybdates are unique in that they are able to absorb molecules into the catalyst bulk, allowing a three-dimensional reaction field [17]. This process is favored by catalysts that contain counter cations with a small radius to charge ratio, e.g. Na^+ , Cu^{2+} and H^+ rather than Cs^+ and NH_4^+ [2]. Heteropoly compounds resemble liquids in the way they absorb such large amounts of gaseous species [18]. This ability of heteropoly substrates to absorb molecules into the bulk allows reactions to proceed with surface area-independent kinetics, that is, surface area does not impact on the reaction rates [17].

About 2.7 million tonnes of methyl methacrylate was produced world-wide, in 2009 [19], with 85% manufactured via the acetone cyanohydrin (ACH) process [20]. This process uses hydrogen cyanide as a feedstock and forms ACH as an intermediate, both of which are highly toxic, and ammonium hydrogen sulfate is coproduced in large quantities, which is contaminated with organics and has to be pyrolyzed or disposed of in spoil banks. Supply shortage of hydrogen cyanide also affects this production method [21]. These deleterious factors have prompted research into environmentally responsible alternatives, and new commercial processes for methyl methacrylate have been developed [21] and include the two step catalytic oxidation of isobutene into methacrylic acid, the methacrylonitrile (MAN) method, the BASF route, modified ACH process (Mitsubishi Chemical Co. Inc.), and the direct oxidative esterification of methacrolein (Asahi Chemical Co. Inc.). Phosphomolybdic acid has been shown to be effective for the selective oxidation of isobutane into methacrolein, and substitution of the protons with copper or lanthanide cations has improved oxidation performance [22–24]. Therefore formation of methacrolein from the oxidation of isobutane by phosphomolybdic acid derivatives may be a viable catalytic solution to the ACH process.

Temperature-programmed reaction spectroscopy (TPRS) is a widely used method for analyzing chemical reactions. Essentially it is the monitoring of reaction processes by

analytic methods whilst the temperature is increased linearly with respect to time. Large temperature fluctuations associated with exothermic adsorption processes can be avoided by establishing equilibrium at low temperatures, whereby negligible reaction occurs. TPRS allows the investigation of a wide range of temperatures in a short period of time and is ideally suited to the determination of kinetic parameters. TPRS may also be used to monitor desorptions. This technique has been employed by Kendell et al. to elucidate accurate kinetic parameters for isobutane selective oxidation over phosphomolybdic acid and different cationic substituted derivatives [22–24]. This paper presents the structural affects of Group 1 and 2 cation addition the phosphomolybdate structure and how this impacts on the selective oxidation of isobutane into various products, but principally methacrolein formation.

2 Experimental

2.1 Sample Preparation

Isobutane and argon were obtained from BOC gases and used without further purification. Metal substituted phosphomolybdates were prepared by addition of metal carbonates to a solution of phosphomolybdic acid, then drying to a solid. The phosphomolybdic acid and other reagents were obtained from Aldrich and used without purification; analysis determined that the phosphomolybdic acid was hydrated with 29 waters per Keggin unit. A typical preparation for $\text{Li}_2\text{H}[\text{PMo}_{12}\text{O}_{40}]$ follows: 10.3196 g of phosphomolybdic acid was dissolved in ~40 mL of water with stirring. 0.3273 g of Li_2CO_3 was added with continued stirring (evolution of carbon dioxide). The solution was heated to about 60 °C with stirring until thick slurry was produced. Drying was completed by placing in an oven at 120 °C overnight. Solid $\text{Li}_2\text{H}[\text{PMo}_{12}\text{O}_{40}]$ was ground and stored in preparation for TPRS experiments.

Group 1 compounds were of the form $\text{M}_x\text{H}_{3-x}[\text{PMo}_{12}\text{O}_{40}]$, where $\text{M} = \text{Li}, \text{Na}, \text{K}, \text{Rb}$ or Cs , and $x = 1, 2$ and 3, and also 2.5 for Cs ; the Group 2 compounds were of the form $\text{M}_x\text{H}_{3-2x}[\text{PMo}_{12}\text{O}_{40}]$, where $\text{M} = \text{Mg}, \text{Ca}, \text{Sr}$ or Ba , and $x = 0.5, 1$ and 1.5.

2.2 X-Ray Diffraction (XRD)

The phosphomolybdates were analyzed via XRD using the facilities at James Cook University, Australia. Powdered XRD measurements were performed on a D5000 Diffractometer, equipped with a copper anode X-ray tube. The radiation used for the analysis consisted of $\text{Cu K}\alpha$ X-rays with a wavelength of 154.06 pm. Samples were systematically scanned with 2θ angles ranging from 1.3° to 65.3°,

using 0.02° increments. Past investigations have demonstrated that the XRD data of phosphomolybdic acid is modified depending upon extent of hydration [6, 15]. For this reason, all samples were uniformly calcined at 300 °C for 4 h, prior to being sent off for analysis.

2.3 Experimental Apparatus and Technique for TPRS

A low-pressure steady-state apparatus has been constructed in order to analyze reactions using the TPRS technique. This apparatus has been described previously [22–24]. Briefly, reactions were conducted in a Pyrex Knudsen cell reactor, which contained approximately 1.5 g (accurately weighed) of the solid samples. Prior to initiating experiments, samples were pretreated under vacuum in the Knudsen cell at 200 °C for about 24 h to remove the majority of water, and residual carbonates. A reactant feed-stream of an equimolar mixture of isobutane and argon was used (oxygen was not included in the feed stream, instead oxidations were facilitated by lattice oxygen in the substrate, consistent with a Mars-van Krevelen mechanism [25]). The feed stream is flowed into the Knudsen cell reactor, with the flow restricted to less than 10^{15} molecules per second and reactor pressure maintained between 7–10 Pa; this ensured a molecular flow regime in which gas-phase collisions were minimized and secondary reactions prevented [24]. Oxidation products, argon and unreacted isobutane exited the Knudsen cell through an aperture and passed directly into a quadrupole mass spectrometer. The theory of heterogeneous reactions in a Knudsen cell have been detailed previously [24, 26].

The reactor was enclosed in a temperature-programmable furnace. Each sample was subjected to five temperature-programmed experiments. The first experiments with each phosphomolybdate tend to yield poor quality data due to the occupation of active sites by water and other molecules [24], therefore these initial runs function as an additional pretreatment procedure. TPRS for each compound was conducted from 100 °C to a maximum of 400 °C (for the first experiment) or 500 °C (for the subsequent four experiments), at a heating rate of 5 °C min⁻¹. Decomposition of phosphomolybdic acid occurs at temperatures above 400 °C [11, 27–29], so the lower maximum temperature for the initial TPRS experiment allowed for elimination of water and other molecules from the phosphomolybdates, whilst ensuring thermal degradation of the Keggin framework does not occur before useful selective oxidation data can be obtained. It should be noted however, the addition of cations to the phosphomolybdate anion enhances thermal stability significantly [12, 30–32], so the termination of the first experiment at 400 °C is a conservative

precaution; indeed, kinetic investigation into the Group 1 and 2 salts has shown no evidence of degradation with the later experiments with ca. 500 °C maximums (*vide infra*). Kendall et al. have conducted IR analyses on similar phosphomolybdates before and after TPRS and the structure was preserved [22].

Prior to each experiment the reactant feed stream was flowed for ca. 2 h. This allowed for a steady-state to be established. The first four experiments were then conducted whilst maintaining this steady-state flow. The fifth experiments differed: the steady-state regime is established in the hour or so preceding, however 20 min prior to commencement of the fifth experiments, the reactant flow was turned off and the cell was evacuated for 20 min. This allowed for elimination of gas-phase isobutane, and the products formed during TPRS were from reaction of adsorbed isobutane only. Aside from this, the temperature ramp and data acquisition process remained the same as the previous four experiments.

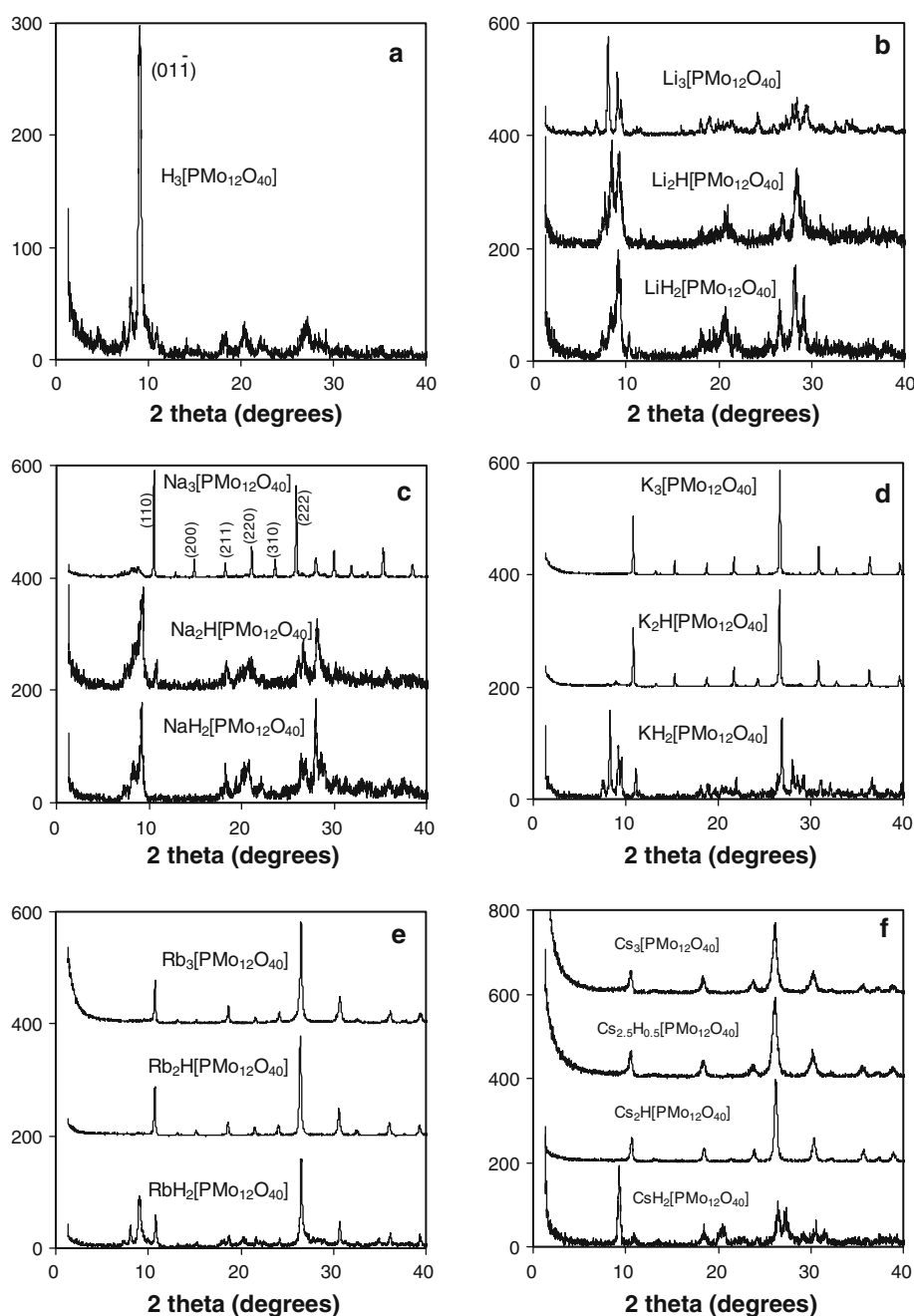
3 Results and Discussion

3.1 XRD Analysis

The XRD investigation showed that all the phosphomolybdates exhibit a crystalline structure, however there is a wide variation amongst the X-ray spectra, and hence variation in the unit cells and lattices. The structure of phosphomolybdic acid consists of a triclinic phase, as previously discussed by Langpape et al. [6]. Past investigations have demonstrated that the XRD data of phosphomolybdic acid is modified depending upon extent of hydration [6, 15]. For this reason, all samples were uniformly calcined at 300 °C for 4 h, prior to being sent off for analysis. The powdered XRD pattern for phosphomolybdic acid is given in Fig. 1a. Pure phosphomolybdic acid exists in a triclinic phase. The maximum peak shown in Fig. 1a occurs at $2\theta = 9.06$ and corresponds to the (01 $\bar{1}$) lattice plane.

The extent of hydration significantly affects the XRD patterns. Previous work by Langpape et al. has been published which shows the XRD data for phosphomolybdic acid and cesium phosphomolybdates with varying degrees of hydration [6]. Comparison of the diffraction pattern of phosphomolybdic acid (calcined at 300 °C for 4 h) with the work from Langpape et al. suggests that the extent of hydration of the pure acid is 13 water molecules per Keggin unit, and therefore the acid used for the X-ray work in this study is assumed to be H₃[PMo₁₂O₄₀]·13H₂O. It should be noted, however, that the 300 °C calcinations render the samples completely anhydrous and that the 13 water molecules per H₃[PMo₁₂O₄₀] are the result of

Fig. 1 XRD spectra for pure phosphomolybdic acid (a) and the lithium (b), sodium (c), potassium (d), rubidium (e) and cesium (f) phosphomolybdate series



rehydration of the sample prior to analysis. Moreover, the first TPRS removes any rehydration water that results from handling the samples, hence all kinetically relevant TPRS experiments are conducted on anhydrous phosphomolybdates.

3.1.1 Group 1 Phosphomolybdates

Substitution of the protons by the alkali cations causes a change in the spectra dependent upon the cation used and the extent of replacement. The addition of lithium to the phosphomolybdate anion causes significant structural

effects, as compared to the pure acid. The large (011) peak from the triclinic phase becomes distorted with the first replacement of a proton with a lithium cation. The peak partially separates with the second substitution and finally forms two distinct peaks with $\text{Li}_3[\text{PMo}_{12}\text{O}_{40}]$ (Fig. 1b). This is evidence of another phase being present along with the triclinic phase.

Sodium addition to the phosphomolybdate framework results in X-ray spectra that are very different to that of the pure acid, and these are given in Fig. 1c. The lower substituted $\text{NaH}_2[\text{PMo}_{12}\text{O}_{40}]$ and $\text{Na}_2\text{H}[\text{PMo}_{12}\text{O}_{40}]$ compounds display peaks that are not clearly defined, which is

likely due to the presence of the triclinic phase. The fully substituted $\text{Na}_3[\text{PMo}_{12}\text{O}_{40}]$ salt, however, shows clearly resolvable XRD peaks. This is due to the presence of a body centered cubic phase. Several peaks of the $\text{Na}_3[\text{PMo}_{12}\text{O}_{40}]$ diffraction pattern, given in Fig. 1c, have been labeled with the Miller indices associated with the cubic structure.

The addition of potassium to the phosphomolybdate structure is associated with the appearance of the body centered cubic phase. The body centered cubic character is apparent in the $\text{KH}_2[\text{PMo}_{12}\text{O}_{40}]$ diffraction pattern, however the peaks are complicated. In comparison, $\text{K}_2\text{H}[\text{PMo}_{12}\text{O}_{40}]$ and $\text{K}_3[\text{PMo}_{12}\text{O}_{40}]$ display well resolved spectra, consistent with body centered cubic structures, and there is little evidence of another phase being present. Figure 1d shows a comparison of the three potassium compound spectra. Clearly seen for the $\text{KH}_2[\text{PMo}_{12}\text{O}_{40}]$ pattern, are peaks at about 11° and 27° on the 2θ axis. These correspond to peaks in the $\text{K}_2\text{H}[\text{PMo}_{12}\text{O}_{40}]$ and $\text{K}_3[\text{PMo}_{12}\text{O}_{40}]$ spectra. This demonstrates that a partial body centered cubic phase is established with the mono-substituted potassium salt, however, another phase is responsible for the poorly resolved pattern.

All rubidium and cesium compounds exhibit a body centered cubic phase, as shown in Fig. 1e and f, respectively. However, these figures demonstrate that there is still a significant contribution from another phase for the mono-substituted rubidium and cesium salts; $\text{RbH}_2[\text{PMo}_{12}\text{O}_{40}]$ has three peaks below $2\theta = 10^\circ$ and $\text{CsH}_2[\text{PMo}_{12}\text{O}_{40}]$ exhibits a large spike at $2\theta = 9^\circ$.

3.1.2 Factors Affecting Structure of Group 1 Phosphomolybdates

A previous study by Black et al. has identified the presence of multiple phases for the potassium phosphomolybdates [15] and Christian and Whittingham have observed the presence of multiple cubic structures [33]. The catalysts investigated were of the form $\text{K}_x\text{H}_{3-x}[\text{PMo}_{12}\text{O}_{40}]$, where $x = 0, 0.5, 1, 1.5, 2, 2.5, 2.75$ and 3 . This study showed that diffraction patterns of catalysts with intermediate composition ($0.5 \leq x \leq 2.0$) consist of more than one phase, while the heavier substituted ($2.0 \leq x \leq 3.0$) catalysts possess the $\text{K}_3[\text{PMo}_{12}\text{O}_{40}]$ phase exclusively. Figure 1d shows that the mono-substituted potassium salt ($\text{KH}_2[\text{PMo}_{12}\text{O}_{40}]$) has a mixture of cubic and another phase, whereas the doubly- and triply-substituted compounds ($\text{K}_2\text{H}[\text{PMo}_{12}\text{O}_{40}]$ and $\text{K}_3[\text{PMo}_{12}\text{O}_{40}]$) essentially exhibit only the body centered cubic structure. A close examination of Fig. 1d, however, identifies two small peaks below $2\theta = 10^\circ$ for the $\text{K}_2\text{H}[\text{PMo}_{12}\text{O}_{40}]$ compound that are not consistent with a body centered cubic structure. These peaks are evidence that another phase is present

alongside the cubic phase, albeit in small measure. Black et al. has shown that XRD data is heavily dependent upon the extent of hydration [15]. The potassium phosphomolybdates investigated by Black et al. [15] were calcined at 400°C , whereas those analyzed in this work were prepared at 300°C . However, past about 150°C all water of hydration should be removed so the discrepancy is most likely attributed to rehydration of our sample prior to analysis.

Other, more recent analyzes have been reported by Hu and Burns [34] and Langpape et al. [6] with cesium derivatives, of varying compositions of the form $\text{Cs}_x\text{H}_{3-x}[\text{PMo}_{12}\text{O}_{40}]$. These have shown that for $x < 2$, two distinct phases are observed in XRD patterns, while for $x \geq 2$ only the cubic phase is detectable. These findings agree with the results obtained by Black et al. [15] and with those reported above. Further investigation by Langpape et al. [6] has shown evidence that for cesium phosphomolybdates with substitution greater than or equal to two cesium atoms per Keggin unit, there exists $\text{Cs}_3[\text{PMo}_{12}\text{O}_{40}]$ particles thinly coated by pure $\text{H}_3[\text{PMo}_{12}\text{O}_{40}]$. This finding is supported by related work conducted on cesium phosphotungstates by Misono, where he has shown that particles of $\text{Cs}_3[\text{PW}_{12}\text{O}_{40}]$ form with $\text{H}_3[\text{PW}_{12}\text{O}_{40}]$ filling the interstices of the $\text{Cs}_3[\text{PW}_{12}\text{O}_{40}]$ crystallites [2]. For cesium salts with two or more cesium atoms per Keggin unit, the coating of pure acid on the fully substituted cesium phosphomolybdate particles may not be detected by XRD, hence only the body centered cubic phase may be apparent for these salts. This effect is most likely responsible for Black et al. [15] observing exclusive cubic phases in the potassium salts with two or more potassium cations per Keggin unit. Rubidium is between potassium and cesium in the periodic table, and therefore it intuitively follows that the structural trends of the phosphomolybdates made from this alkali metal are consistent with the results for the potassium and cesium derivatives.

Table 1 shows a comparison of the effective ionic radii [35] of the different Group 1 cations, all radii refer to the cation in a six coordination state. The coordination state is likely higher than six, however there is no structural data to indicate the exact coordination number. Also shown in this table are the volumes for one, two or three cations of each species. Volumes were determined using the spherical volume relationship $V = (4/3)\pi r^3 n$, where r refers to the ionic radius and n is the number of cations. These values refer to the Group 1 cation volume contribution to a particular phosphomolybdate, e.g. the rubidium cations from $\text{Rb}_2\text{H}[\text{PMo}_{12}\text{O}_{40}]$ contribute a volume of 29.4 \AA^3 . The bold volumes indicate the phosphomolybdates that display a resolvable body centered cubic structure. As this table shows, the cubic character is associated with those phosphomolybdates possessing a Group 1 cationic volume

greater than or equal to 11.0 \AA^3 (Group 1 volume contribution for $\text{KH}_2[\text{PMo}_{12}\text{O}_{40}]$). The greatest cationic volume without cubic character is 8.89 \AA^3 ($\text{Na}_2\text{H}[\text{PMo}_{12}\text{O}_{40}]$). Therefore it may be inferred that the minimum Group 1 cationic volume required to induce a cubic phase is between 9 and 11 \AA^3 . Because the coordination number is likely greater than six, these volumes are not exact, but instead give an approximation of the cationic volume required to form the cubic phase. In any case, the volumes can be used to make a relative comparison of Group 1 cations. Other factors may determine predisposition of phosphomolybdates toward cubic character as a whole, however this relationship holds well for the Group 1 species.

3.1.3 Unit Cell Dimensions

Shown in Table 2 are unit cell dimensions as determined in this work and from previous publications. These values differ from those obtained in this work, however the general trends are the same, with the exception of Langpape et al. reporting a larger unit cell for $\text{Cs}_3[\text{PMo}_{12}\text{O}_{40}]$ than for $\text{Cs}_{2.5}\text{H}_{0.5}[\text{PMo}_{12}\text{O}_{40}]$. The generally larger unit cell dimensions are probably due to differing extents of hydration. The samples were calcined at $350 \text{ }^\circ\text{C}$ for 5 h by Langpape et al. [6], at $300 \text{ }^\circ\text{C}$ for 6 h by Hu and Burns [34] and at $300 \text{ }^\circ\text{C}$ for 4 h for this work. Unit cell dimensions for non-cubic phases observed from the XRD data were unable to be determined.

3.1.4 Group 2 Phosphomolybdates

The XRD patterns for the Group 2 phosphomolybdates are quite different from their Group 1 analogues. There is no evidence of a cubic phase with any of the divalent cation derivatives, instead the triclinic phase associated with the Group 1 compounds is maintained. XRD data for the magnesium compounds analyzed in this work is given in Fig. 2a. The location of the peaks correlates closely to

previous XRD analyzes on phosphomolybdic acid [6] with the peak positions at around 8.2° and 9.2° being indicative of the respective (110) and (01 $\bar{1}$) planes of a triclinic phase. These peaks are visible for all the magnesium derivatives, but the $\text{Mg}_{1.5}[\text{PMo}_{12}\text{O}_{40}]$ displays a weaker (110) contribution than the other salts. There are however, peaks in the spectra that are not accounted for by triclinic phases and so there are other phases present, although no evidence of a cubic phase is observed for the magnesium phosphomolybdates. The calcium compounds also exhibit XRD spectra consistent with the presence of triclinic phases, especially the presence of the (01 $\bar{1}$) plane. The contribution from the (110) plane ($\sim 2\theta = 8.3^\circ$) is prominent for $\text{Ca}_{0.5}\text{H}_2[\text{PMo}_{12}\text{O}_{40}]$, however it is quite weak for $\text{CaH}[\text{PMo}_{12}\text{O}_{40}]$ and undetectable in the $\text{Ca}_{1.5}[\text{PMo}_{12}\text{O}_{40}]$ pattern (Fig. 2b). As with the magnesium spectra, there exists an indeterminable phase along with the triclinic component, and no cubic structure is observed. Figure 2c displays the diffraction patterns of the strontium phosphomolybdates. The strontium compounds maintain the (01 $\bar{1}$) plane, while the (110) lattice only appears with $\text{Sr}_{0.5}\text{H}_2[\text{PMo}_{12}\text{O}_{40}]$. The pattern for the fully substituted salt, $\text{Sr}_{1.5}[\text{PMo}_{12}\text{O}_{40}]$, appears to become disordered and may reflect the development of significant amorphous character. As with the previous Group 2 phosphomolybdates, there is no discernable cubic phase associated with the strontium derivatives, and phases other than triclinic contribute to the diffraction data. The barium phosphomolybdates, like the previous Group 2 phosphomolybdates, exhibit the characteristic (01 $\bar{1}$) plane, as shown in Fig. 2d. The (110) lattice plane is non-existent in the heavier substituted $\text{BaH}[\text{PMo}_{12}\text{O}_{40}]$ and $\text{Ba}_{1.5}[\text{PMo}_{12}\text{O}_{40}]$ compounds and is barely resolvable with $\text{Ba}_{0.5}\text{H}_2[\text{PMo}_{12}\text{O}_{40}]$. The spectra of $\text{BaH}[\text{PMo}_{12}\text{O}_{40}]$, and $\text{Ba}_{1.5}[\text{PMo}_{12}\text{O}_{40}]$ in particular, are disordered and may reflect a substantial amorphous component in these solids. As with the other Group 2 phosphomolybdates, there is more than the triclinic phase associated with each of the barium containing solids, and a cubic phase is not present.

Table 1 Comparison of effective ionic radii and volumes for the Group 1 cations used for the synthesis of the phosphomolybdates in this work

Cation	Effective ionic radius (\AA)	Effective ionic volume (\AA^3)		
		Single cation	Double cation	Triple cation
Li^+	0.76	1.84	3.68	5.52
Na^+	1.02	4.45	8.89	13.3
K^+	1.38	11.0	22.0	33.0
Rb^+	1.52	14.7	29.4	44.1
Cs^+	1.67	19.5	39.0	58.5

The single, double and triple cation columns refer to the respective effective volumes occupied by one, two or three cations. The bold volumes correspond to the phosphomolybdates exhibiting a resolvable body centered cubic structure. Effective ionic radii data obtained from previous work by Shannon [35]

Table 2 Unit cell dimensions for those Group 1 catalysts possessing the body centered cubic phase

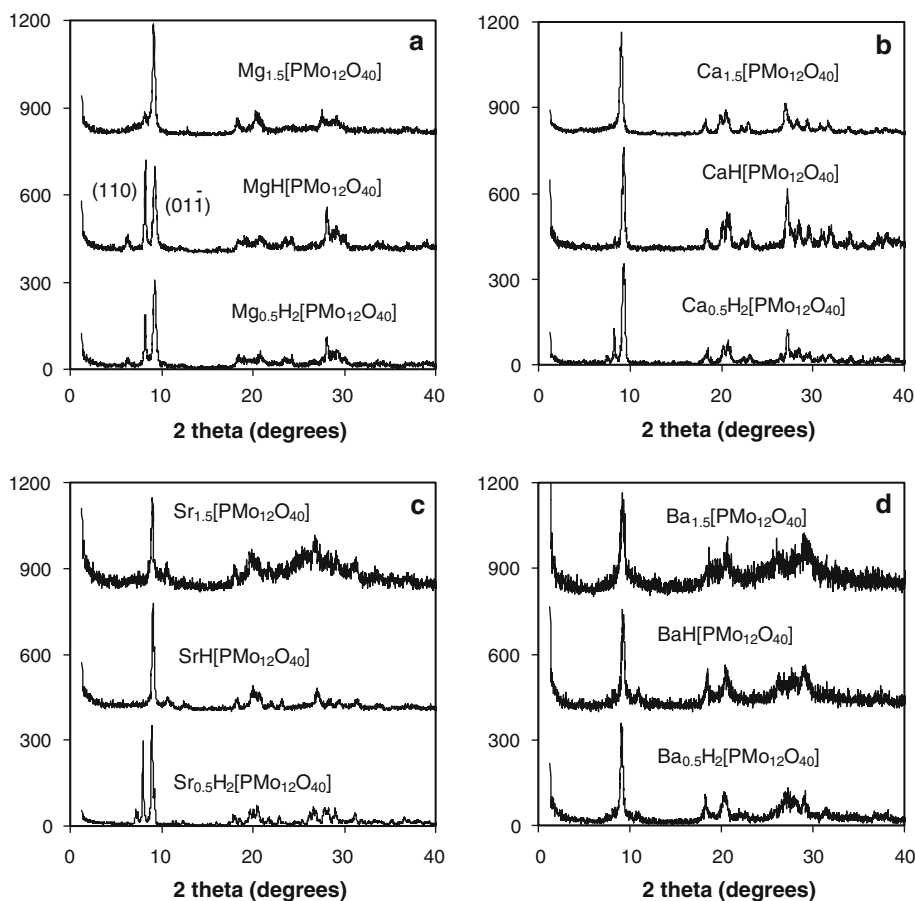
Compound	a (Å)		
	This work	Hu and Burns [34]	Langpape et al. [6]
Na ₃ [PMo ₁₂ O ₄₀]	11.882 (2)	11.936 (1)	–
KH ₂ [PMo ₁₂ O ₄₀]	11.476 (4)	–	–
K ₂ H[PMo ₁₂ O ₄₀]	11.568 (10)	–	–
K ₃ [PMo ₁₂ O ₄₀]	11.571 (7)	11.5975 (2)	–
RbH ₂ [PMo ₁₂ O ₄₀]	11.632 (7)	–	–
Rb ₂ H[PMo ₁₂ O ₄₀]	11.681 (11)	–	–
Rb ₃ [PMo ₁₂ O ₄₀]	11.642 (6)	11.6687 (5)	–
CsH ₂ [PMo ₁₂ O ₄₀]	11.671 (20)	–	11.819 (8)
Cs ₂ H[PMo ₁₂ O ₄₀]	11.763 (11)	–	11.820 (7)
Cs _{2.5} H _{0.5} [PMo ₁₂ O ₄₀]	11.829 (4)	–	11.825 (5)
Cs ₃ [PMo ₁₂ O ₄₀]	11.810 (3)	11.8412 (9)	11.828 (6)

3.1.5 Discussion of Group 2 Phosphomolybdate

XRD Data

Clearly resolvable triclinic phases are present for the Group 2 phosphomolybdates, with characteristic peaks given by the (110) and (01 $\bar{1}$) lattice planes. There is a trend with

Fig. 2 XRD patterns for the magnesium (a), calcium (b), strontium (c) and barium (d) phosphomolybdates analyzed in this work



larger cation substitution diminishing the intensity of the (110) peak, however this seems to have little impact on the (01 $\bar{1}$) peak. A similar phenomenon has been observed with other heteropoly compounds and the contribution of the (110) is thought to be related to the micropore volume of the solids [8, 9, 13]. The larger cations also appear to introduce disorder and possibly amorphousness. Table 3 shows the relationship between volume of the divalent cations and absence of the (110) peak. The effective ionic radii data was obtained from previous work by Shannon [35] and each of the values is for the cation in a six coordination state. The bold volumes in Table 3 show the volumes of those phosphomolybdates which do not possess the (110) plane. This corresponds to compounds with Group 2 cation volumes of 6.28 Å³ (representing Ca_{1.5}[PMo₁₂O₄₀]) or greater. The lowest alkaline cation volume contribution that would result in absence of the (110) plane is somewhere between 5 and 6 Å³ (Ba_{0.5}H₂[PMo₁₂O₄₀] and Ca_{1.5}[PMo₁₂O₄₀]). As in the case of the Group 1 cations the volumes are not absolute, but they approximate the required volume and may be used for relative comparisons.

The fully substituted magnesium, calcium, strontium and barium salts (Mg_{1.5}[PMo₁₂O₄₀], Ca_{1.5}[PMo₁₂O₄₀], Sr_{1.5}[PMo₁₂O₄₀] and Ba_{1.5}[PMo₁₂O₄₀]), have been prepared and

analyzed by McGarvey and Moffat [16]. The publication reported that the XRD data of the divalent compounds was “largely featureless”. These authors concluded that the preparation methods they employed did not result in alkaline earth phosphomolybdates, but rather a mixture of phosphomolybdic acid and a divalent salt. This is likely to be due to the use of hydroxides in the synthetic method, which raise the preparatory solution pH; the Keggin structure is only stable at pH values less than 1.5 [36] and is rapidly and completely destroyed at a pH value of 4 [37]. The phosphomolybdates in this work were not prepared using alkaline earth hydroxides and therefore the triclinic XRD patterns are observed.

Silviani and Burns [12] have also investigated the diffraction spectra of the alkaline earth phosphomolybdates. In contrast to the results presented here, Silviani and Burns [12] observed only a cubic structure without evidence of any amorphous or other phases (including triclinic). The synthesis of the compounds was analogous to the method used in this thesis, so it is unlikely that a synthetic anomaly is responsible for the different X-ray spectra. A significant difference lies in the way the samples were prepared prior to analysis; Silviani and Burns [12] did not calcine the solids in any way and tried to prevent samples from losing water, whereas the compounds in this work were taken to 300 °C for 4 h. The different sample pre-treatments cause vastly different hydration extents and as outlined previously [15]. This is associated with very different XRD spectra and may explain the discrepancy between this work and that published by Silviani and Burns [12].

3.2 Products from TPRS

Products observed from the reaction of isobutane with phosphomolybdic acid using this technique were methacrolein, 3-methyl-2-oxetanone (lactone), acetic acid, carbon dioxide and water; these selective oxidation products for isobutane over phosphomolybdic acid have been previously reported by Kendell and coworkers [23, 24]. Products observed over the Group 1 and 2 phosphomolybdates are also methacrolein, lactone, acetic acid, carbon dioxide and

water. However propene forms over some of the Group 1 salts (but not over Group 2 compounds) and methacrylic acid is also seen over a single Group 2 phosphomolybdate: BaH[PMo₁₂O₄₀]. It has been shown that lactone is a precursor to methacrylic acid, and the lactone is prevented from rearranging into methacrylic acid due to the unique low-pressure, steady-state, molecular flow conditions used in TPRS [38]. Interestingly, the cesium series of phosphomolybdates were the compounds that did not produce any lactone or acetic acid, and only minimal CO₂, but were very active toward methacrolein formation. Therefore cesium addition has yields highly selective oxidation substrates. Carbon dioxide and water are not products of interest and it can be difficult to quantify their quantities, hence they have been excluded from further analysis.

3.2.1 Distributions

Two types of distributions were identified, designated as Category 1 and Category 2:

Category 1: Distributions where formation increases with increasing temperature, in a manner consistent with an exponential product evolution and are only observed whilst gas-phase isobutane is present.

Category 2: Profiles that consist of several rises, falls and inflections (although sometimes a single peak is observed), usually overlapping and only resolvable into individual peaks by extensive modeling using Gaussian curves; this type of distribution is observed with or without gas-phase isobutane flowing over the substrate.

3.2.2 Resolution of Category 2 Peaks

The Category 2 profiles are complicated, but nonetheless they are experimentally reproducible and form consistently. It is assumed that the convoluted nature of the Category 2 product formation is due to the concurrent desorption of product from different distinct active sites within the phosphomolybdate, with each site exhibiting

Table 3 Comparison of effective ionic radii and volumes for the Group 2 cations used for the synthesis of the phosphomolybdates in this work

Cation	Effective ionic radius (Å)	Effective ionic volume (Å ³)		
		0.5 cation	1 cation	1.5 cation
Mg ²⁺	0.72	0.78	1.56	2.35
Ca ²⁺	1.00	2.09	4.19	6.28
Sr ²⁺	1.18	3.44	6.88	10.3
Ba ²⁺	1.35	5.15	10.3	15.5

The 0.5, 1 and 1.5 cation columns refer to the respective effective volumes occupied by 0.5, 1 and 1.5 cations. The bold volumes correspond to the phosphomolybdates that do not exhibit a resolvable (110) triclinic lattice plane. Effective ionic radii data obtained from previous work by Shannon [35]

unique kinetic parameters. Previous researchers have simulated temperature-programmed desorption using Gaussian curves and used these to determine thermodynamic parameters [39–42]. The mass spectral intensities in this work, I_p , are a function of temperature, T . I_p is simulated by the following Gaussian expression [23, 43]:

$$I_p = h \exp\left(\frac{-(T-p)^2}{2w^2}\right) \quad (1)$$

The parameters h and p determine respective peak height and position, while w alters the peak width. Usually, multiple Gaussian curves are required to adequately simulate the experimental data, with parameters for each curve optimized via a non-linear least squares analysis of their summation.

Methacrolein forms via Category 1 and 2 processes, with all other products forming as Category 2 distributions. Figure 3 shows the smooth exponential rise associated with Category 1 methacrolein formation over the $\text{KH}_2[\text{PMo}_{12}\text{O}_{40}]$ salt. Figure 4 is lactone formation over $\text{Mg}_{1.5}[\text{PMo}_{12}\text{O}_{40}]$; the experimental data has been simulated by two Gaussian distributions.

Tables 4 and 5 show the products formed over the Group 1 and 2 phosphomolybdates respectively. The abbreviations MA, LAC, AA, PE and MAA designate methacrolein, lactone, acetic acid, propene and methacrylic acid respectively. The “MA Cat. 1” column indicates with a Y if Category 1 methacrolein formation was observed and a dash if not. The columns to the right of this detail how many Category 2 desorption peaks are associated with each species; e.g. for selective oxidation of isobutane over $\text{LiH}_2[\text{PMo}_{12}\text{O}_{40}]$, Category 1 methacrolein was observed and there were four Category 2 methacrolein desorption

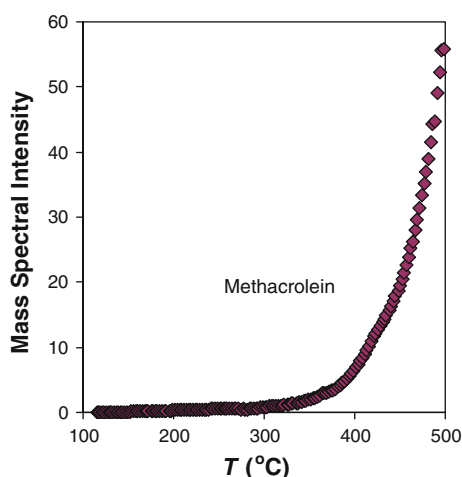


Fig. 3 Methacrolein production from isobutane anaerobic oxidation over $\text{KH}_2[\text{PMo}_{12}\text{O}_{40}]$

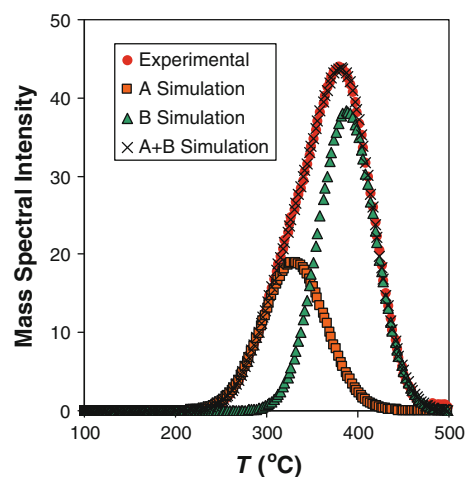


Fig. 4 Lactone experimental data for isobutane oxidation over $\text{Mg}_{1.5}[\text{PMo}_{12}\text{O}_{40}]$. The experimental data is simulated by applying two separate distinct Gaussian distributions

peaks, four lactone desorptions, three acetic acid desorptions and no propene desorptions.

3.2.3 Detection of Methacrylic Acid

Methacrylic acid has been shown to form from the oxidation of isobutane over heteropoly compounds such as phosphomolybdates [7, 44–50]. Typically, methacrylic acid is not formed for isobutane selective oxidation with the low-pressure TPRS system employed in this study [22–24]. This is because the molecular flow conditions

Table 4 Products associated with the anaerobic oxidation of isobutane over phosphomolybdates containing metals from Group 1 of the periodic table

Catalyst	MA Cat. 1	MA Cat. 2	LAC	AA	PE
$\text{LiH}_2[\text{PMo}_{12}\text{O}_{40}]$	Y	4	4	3	–
$\text{Li}_2\text{H}[\text{PMo}_{12}\text{O}_{40}]$	–	7	6	4	–
$\text{Li}_3[\text{PMo}_{12}\text{O}_{40}]$	–	1	1	–	–
$\text{NaH}_2[\text{PMo}_{12}\text{O}_{40}]$	–	4	4	–	–
$\text{Na}_2\text{H}[\text{PMo}_{12}\text{O}_{40}]$	–	5	5	–	5
$\text{Na}_3[\text{PMo}_{12}\text{O}_{40}]$	–	4	–	–	3
$\text{KH}_2[\text{PMo}_{12}\text{O}_{40}]$	Y	7	6	–	–
$\text{K}_2\text{H}[\text{PMo}_{12}\text{O}_{40}]$	–	6	4	6	–
$\text{K}_3[\text{PMo}_{12}\text{O}_{40}]$	–	6	3	–	–
$\text{RbH}_2[\text{PMo}_{12}\text{O}_{40}]$	–	6	4	5	–
$\text{Rb}_2\text{H}[\text{PMo}_{12}\text{O}_{40}]$	Y	–	3	4	–
$\text{Rb}_3[\text{PMo}_{12}\text{O}_{40}]$	–	5	3	–	6
$\text{CsH}_2[\text{PMo}_{12}\text{O}_{40}]$	Y	2	–	–	–
$\text{Cs}_2\text{H}[\text{PMo}_{12}\text{O}_{40}]$	Y	5	–	–	–
$\text{Cs}_{2.5}\text{H}_{0.5}[\text{PMo}_{12}\text{O}_{40}]$	Y	–	–	–	–
$\text{Cs}_3[\text{PMo}_{12}\text{O}_{40}]$	Y	2	–	–	–

Table 5 Products associated with the anaerobic oxidation of isobutane over phosphomolybdates containing metals from Group 2 of the periodic table

Catalyst	MA Cat. 1	MA Cat. 2	LAC	AA	MAA
Mg _{0.5} H ₂ [PMo ₁₂ O ₄₀]	Y	4	5	–	–
MgH[PMo ₁₂ O ₄₀]	Y	5	5	5	–
Mg _{1.5} [PMo ₁₂ O ₄₀]	Y	5	2	–	–
Ca _{0.5} H ₂ [PMo ₁₂ O ₄₀]	Y	4	5	4	–
CaH[PMo ₁₂ O ₄₀]	Y	5	5	–	–
Ca _{1.5} [PMo ₁₂ O ₄₀]	Y	4	3	6	–
Sr _{0.5} H ₂ [PMo ₁₂ O ₄₀]	–	7	6	5	–
SrH[PMo ₁₂ O ₄₀]	Y	4	4	–	–
Sr _{1.5} [PMo ₁₂ O ₄₀]	–	5	5	–	–
Ba _{0.5} H ₂ [PMo ₁₂ O ₄₀]	Y	6	3	6	–
BaH[PMo ₁₂ O ₄₀]	–	7	6	5	1
Ba _{1.5} [PMo ₁₂ O ₄₀]	–	6	5	7	–

minimize molecule collisions and thus prevent secondary reactions. Previous work by Nguyen et al. has shown that lactone is the precursor to methacrylic acid formation, with the rearrangement catalyzed by water and acid [38]. Surprisingly, methacrylic acid was detected over the BaH[PMo₁₂O₄₀] compound. Observation of this species coincided with rise and fall of a lactone peak, with the lactone and methacrylic acid forming in parallel, as shown in Fig. 5, and indicates that some of the lactone is being converted to methacrylic acid. There are actually six lactone desorption peaks associated with the lactone formation over BaH[PMo₁₂O₄₀], with only the second site being associated with the rearrangement. It is not clear why a single barium substitution facilitates methacrylic acid formation, or why the acid forms in conjunction with the second lactone desorption site only. However, since it has been shown by Nguyen et al. [38] that water and acid catalyze the rearrangement of the lactone into the acid, it may be inferred that the particular site responsible for this rearrangement has water and acid in close proximity.

3.3 Coverage Considerations

The vastly different ways in which Category 1 and 2 products form is due to the way in which isobutane interacts with the phosphomolybdate substrate. Accordingly, these two distributions require significantly dissimilar coverage models to explain product formation.

3.3.1 Category 1 Coverage

The exponential rise associated with the Category 1 distribution is modeled using a Langmuir distribution. This model accurately simulates the experimental data and has

also been used extensively in past investigations [24, 43]. A complete derivation of the theory surrounding the application of Langmuir distributions to the coverage corresponding to low-pressure, molecular flow conditions has been detailed previously [24]; a good first approximation to the reactant fractional coverage for Category 1 (θ_1) is given by the following relationship:

$$\theta_1 = \frac{I_R/\alpha_R}{1 + I_R/\alpha_R + I_P/\alpha_P} \quad (2)$$

Here, I_R and I_P denote the reactant and product mass spectral intensities. The spectral intensities are related to flow rate, in molecules s^{-1} , by α_R and α_P . Figure 6 shows the coverage for the Category 1 distribution of methacrolein over Ba_{0.5}H₂[PMo₁₂O₄₀]. The coverage changes less than 5% during the course of an experiment.

3.3.2 Category 2 Coverage

The Category 2 distributions are a summation of bell-shaped desorptions, as resolved by Gaussian curves. Unlike the Category 1 methacrolein formation, these products rise and concomitantly fall during TPRS. Aside from the intrinsic Arrhenius parameters and temperature, the rate of desorption is determined by the coverage of the desorbing species. At the commencement of TPRS, desorption products are not detected and it is assumed that the fractional coverage at each desorption site is 100%. Likewise, at the completion of TPRS the product formation is negligible and it is supposed that all species have desorbed and the coverage is zero. The Langmuir adsorption isotherm fails to adequately describe the coverage of Category 2 distributions; however the fractional coverage may be

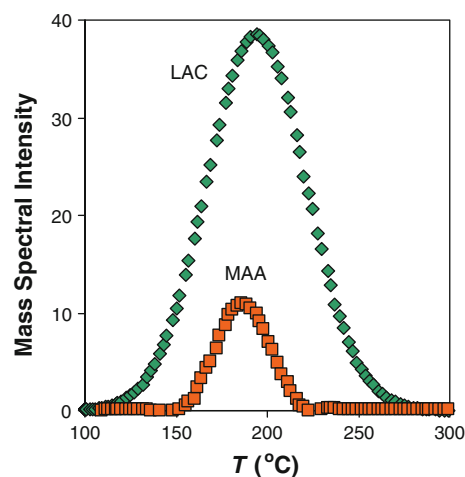


Fig. 5 Gaussian simulations for methacrylic acid formation and the second lactone peak, from isobutane anaerobic oxidation with BaH[PMo₁₂O₄₀]

determined by considering the desorption of the products. Integration of the Gaussian curves yields a fractional desorption function, φ , but antiderivatives for these functions do not exist, so instead the fractional desorption function is determined by the following summation:

$$\varphi = \frac{1}{N} \sum I_P \quad (3)$$

Here N is the total sum of the mass spectral measurements (I_P) and is used to normalize the summation. The fractional coverage of the Category 2 products is then given by:

$$\theta_2 = 1 - \varphi_P = 1 - \frac{1}{N} \sum I_P \quad (4)$$

Figure 7 shows the product profiles (bottom peaks) and coverage functions (top sigmoid curves) for the two lactone distributions observed over $\text{Mg}_{1.5}[\text{PMo}_{12}\text{O}_{40}]$. The coverage functions represent isobutane coverage at each active site for lactone formation. It is important to understand that the coverage terms here represent the coverage of isobutane for each individual active site, rather than considering the isobutane coverage as a whole. This is essential to accurately interpreting the kinetics of each individual product. The coverage changes from unity to essentially zero throughout the TPRS experiment for each Category 2 distribution.

3.4 Kinetic Investigation

A method of simulating of experimental data using low-pressure TPRS technique has been developed [24, 26, 51]. Prior to simulation all data is smoothed using a 25 point quadratic algorithm [52]. The following equation is an

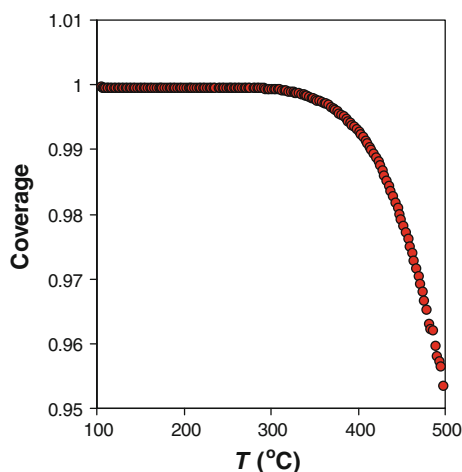


Fig. 6 The fractional coverage of isobutane during reaction with the $\text{Ba}_{0.5}\text{H}_2[\text{PMo}_{12}\text{O}_{40}]$ compound. This figure shows coverage proceeding from unity to approximately 95% during the course of a temperature-programmed experiment

Arrhenius-type expression and has been derived previously [24]:

$$\ln I_P = -\frac{E_{\text{app}}}{RT} + (m+n) \ln \theta + \ln(\beta \alpha_P A_{\text{app}} N(\text{act})^n) \quad (5)$$

This relationship is applicable to the formation of Category 1 products and Category 2 desorption species, whereby the respective θ_1 or θ_2 coverage terms are used for θ in Eq. 4. Here, E_{app} and A_{app} are the respective apparent activation energy and pre-exponential factor, for Category 1 product formation or Category 2 desorptions. The reaction order is given by n , and the parameter m is introduced to correct for any anomalies due to errors in the coverage model or deactivation of the substrate. β is the heating rate and α_P relates the mass spectral intensity to the flux of product molecules. $N(\text{act})$ is the number of active sites available for reaction.

A multiple linear regression analysis is performed with $\ln I_P$ as the Y-input, and $1/RT$ and $\ln \theta$ as the X-inputs; this yields slopes of $-E_{\text{app}}$ and $(m+n)$, and an intercept of $\ln(\beta \alpha_P A_{\text{app}} N(\text{act})^n)$. In practice it can be difficult to ascertain the exact number of active sites available for reaction, particularly where multiple sites are operating independently of each other, so the parameters that constitute the intercept are collectively labeled as A . However, the phosphomolybdates are all derived from phosphomolybdic acid, and hence would have comparable numbers of active sites. Aside from $N(\text{act})$, all other parameters for the intercept are equivalent. Therefore A may be used to make a qualitative relative comparison of the pre-exponential values of the different substrates, rather than in a strictly quantitative manner.

3.4.1 Activity Parameters

Arrhenius parameters were calculated for Category 1 and Category 2 product formations. Methacrolein is the only product to form via a Category 1 profile, whilst Category 2 products include methacrolein, lactone, acetic acid, propene (observed with Group 1 salts) and methacrylic acid (occurring over $\text{BaH}[\text{PMo}_{12}\text{O}_{40}]$ exclusively). The addition of counter cations to the phosphomolybdate structure eliminates Category 1 methacrolein deactivation, hence when conducting a regression analysis on Category 1 methacrolein formation data, $m+n$ in the kinetic model (Eq. 5) was set to unity. Table 6 displays the kinetic parameters determined for Category 1 methacrolein over phosphomolybdates of Groups 1 and 2 respectively. Arrhenius data for the Category 2 distributions is expansive, so rather than list all activation parameters, a range of E_a values for each product is given in Table 7. Unlike the Category 1 distributions, $m+n$ was not unity, rather a value of about 1.3 was universally observed. This likely

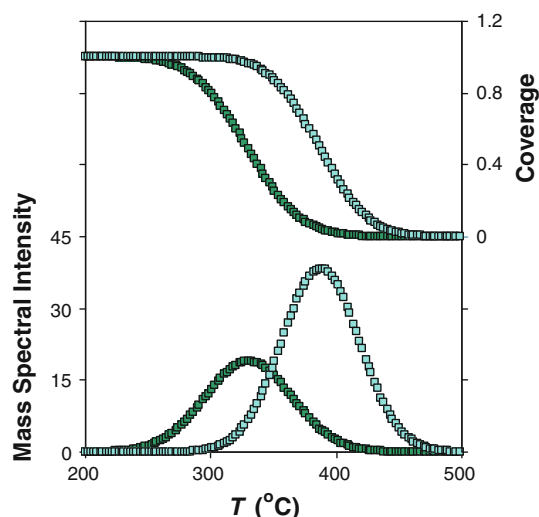


Fig. 7 Fractional coverage of isobutane on $\text{Mg}_{1.5}[\text{PMo}_{12}\text{O}_{40}]$ (top) and corresponding Gaussian product simulations for lactone formation

indicates that the Category 2 products form with an overall reaction order of 1.3. Several samples were resynthesized and reanalyzed using TPRS and very little deviation in kinetic results was observed.

There is great variation among the activation energies associated with the Category 1 and 2 distributions. For Category 1 methacrolein production, $\text{LiH}_2[\text{PMo}_{12}\text{O}_{40}]$ exhibits the lowest activation barrier whilst the fully substituted cesium salt, $\text{Cs}_3[\text{PMo}_{12}\text{O}_{40}]$, has the highest. The Category 2 products show larger variability: the lowest activation barrier is $34.3 \pm 0.4 \text{ kJ mol}^{-1}$ (for the third propene profile over $\text{Rb}_3[\text{PMo}_{12}\text{O}_{40}]$) whilst the highest is $726 \pm 172 \text{ kJ mol}^{-1}$ (occurring with the fourth lactone peak over $\text{KH}_2[\text{PMo}_{12}\text{O}_{40}]$).

3.4.2 Isokinetic Relationship

The kinetic parameters presented in Table 6 show that an increase in E_{app} corresponds to an increase in $\log_{10} A$ for the cesium, magnesium and calcium series. This phenomenon is known as the “compensation effect” or “isokinetic relationship” or and is observed with many reactions [53–65]. Associated with this actuality is a temperature at which the rates of product formation are equivalent, and this is commonly referred to as the “isokinetic temperature” but is also referred to as an “isocatalytic temperature” [57, 58, 62, 63, 65]. Figure 8 shows the Arrhenius plots for Category 1 methacrolein formation over the various cesium salts and the isokinetic temperature. The isokinetic temperature is related to the transition state frequency, ω , and has been derived from stochastic [60], transition-state theory [62, 63, 66] and dynamic [58] models:

$$\omega = \frac{k_{\text{B}}T_{\text{iso}}}{hc} \quad (6)$$

The parameters k_{B} , h and c are Boltzmann, Planck and speed of light constants respectively. Table 8 displays the isokinetic temperature and transition state frequency associated with the cesium, magnesium and calcium compounds. The isokinetic relationship is generally restricted to phosphomolybdates consisting of the same cations. A comparison of Arrhenius plots for phosphomolybdates with differing cations usually does not yield a common point of intersection (isokinetic temperature). For this reason isokinetic points for the cesium, magnesium and calcium phosphomolybdates were individually established. Nevertheless it is interesting to observe that the cesium and magnesium compounds exhibit nearly identical isokinetic temperatures and corresponding transition state frequencies. This connotes that transition states for methacrolein formation over these phosphomolybdates are comparable. Vibrational frequencies for methacrolein were determined using Gaussian 03 software, with calculations performed at the B3LYP/6-31G level. The computational IR frequencies were compared with the actual IR for methacrolein and were in good agreement. The closest frequencies to the values found in Table 8 were ~ 310 and 740 cm^{-1} . These were well outside a 10% error margin. This may indicate that these transition state geometries differ substantially from fully formed methacrolein.

There was no isokinetic relationship observed with any of the Category 2 product formations, e.g. lactone forming over $\text{RbH}_2[\text{PMo}_{12}\text{O}_{40}]$ cannot be compared to that produced over $\text{Rb}_2\text{H}[\text{PMo}_{12}\text{O}_{40}]$ or $\text{Rb}_3[\text{PMo}_{12}\text{O}_{40}]$. This intimates that each Category 2 product forms with unique transition states, even though they belong to the same phosphomolybdate family.

3.5 Reaction Mechanisms

Category 1 is associated with exponential-like distributions and occurs only with methacrolein formation whereas Category 2 profiles are observed with methacrolein, lactone, acetic acid, propene and methacrylic acid (carbon dioxide and water were excluded from modeling). Therefore Category 1 methacrolein formation is likely to occur via a different mechanism from the Category 2 products. None of the Category 2 methacrolein, lactone, acetic acid and propene distributions mirror one another, and there is no other clear relationship between the two, such as number of peaks and temperature positions. Hence it is likely that each has a separate reaction pathway and may involve unique active sites. The methacrylic acid formation displayed by the $\text{BaH}[\text{PMo}_{12}\text{O}_{40}]$ compound matches one

Table 6 Arrhenius parameters for Category 1 methacrolein formation via isobutane anaerobic oxidation with various Group 1 metal phosphomolybdates

Catalyst	E_{app} (kJ mol ⁻¹)	log ₁₀ A	Modeling <i>T</i> Range (°C)
LiH ₂ [PMo ₁₂ O ₄₀]	34.7 (1.3)	4.57 (0.13)	389–478
KH ₂ [PMo ₁₂ O ₄₀]	92 (2)	8.0 (0.2)	428–486
Rb ₂ H[PMo ₁₂ O ₄₀]	64.0 (1.6)	6.71 (0.05)	355–437
CsH ₂ [PMo ₁₂ O ₄₀]	93 (5)	9 (1)	290–372
Cs ₂ H[PMo ₁₂ O ₄₀]	72 (1)	7.5 (0.1)	347–417
Cs _{2.5} H _{0.5} [PMo ₁₂ O ₄₀]	106.1 (1.6)	9.96 (0.15)	342–444
Cs ₃ [PMo ₁₂ O ₄₀]	119 (4)	10.9 (0.8)	370–434
Mg _{0.5} H ₂ [PMo ₁₂ O ₄₀]	70.9 (0.7)	6.62 (0.06)	355–468
MgH[PMo ₁₂ O ₄₀]	67 (2)	6.3 (0.1)	412–497
Mg _{1.5} [PMo ₁₂ O ₄₀]	88.6 (1.1)	7.89 (0.08)	365–466
Ca _{0.5} H ₂ [PMo ₁₂ O ₄₀]	84.5 (1.1)	7.90 (0.08)	402–475
CaH[PMo ₁₂ O ₄₀]	88.7 (1.1)	8.30 (0.08)	367–453
Ca _{1.5} [PMo ₁₂ O ₄₀]	72 (2)	6.7 (0.1)	440–476
SrH[PMo ₁₂ O ₄₀]	50.3 (0.7)	5.96 (0.05)	422–478
Ba _{0.5} H ₂ [PMo ₁₂ O ₄₀]	94.6 (0.4)	8.57 (0.03)	326–479

of the lactone profiles, hence it is proposed that lactone is an intermediate for methacrylic acid.

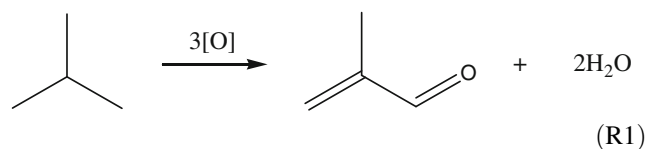
Previous studies have proposed that isobutene acts as an intermediate for methacrolein and methacrylic acid production [46, 50, 67–69], although other authors dispute this claim [70–72]. Similarly, some studies indicate that methacrolein is an intermediate in the formation of methacrylic acid [45, 49, 69], while others give evidence negating this finding [70, 72, 73]. Previous work has indeed shown methacrolein and methacrylic acid production from respective isobutene and methacrolein oxidations over heteropoly compounds [20, 71, 74–77]. However, the discussion of intermediate formation rests on whether either isobutane forms methacrolein and methacrylic acid in one-step oxidations, or respective isobutene- and methacrolein-like intermediary species are involved in a multi-step pathway. The low-pressure, steady-state equipment used for product analysis is very sensitive and the molecular flow conditions minimize secondary collisions which is conducive to isolating intermediates. Nevertheless, isobutene was not detected over any of the phosphomolybdates, hence there is little support for isobutene acting as an intermediate in methacrolein formation from isobutane oxidation. Hence a conclusion from this work is that the oxidation of isobutane into methacrolein occurs via a single step (contemporaneous dehydrogenation and oxygen addition).

Considering the evidence of lactone acting as a precursor to methacrylic acid, and no clear relationship

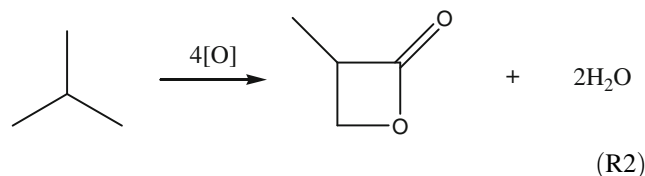
existing between methacrolein and lactone, it may also be concluded that methacrolein does not act as an intermediate for methacrylic acid production. Therefore methacrylic acid is proposed to form via an initial one-step oxidation of isobutane into lactone and a subsequent rearrangement of the lactone.

Propene formation does not correspond to the evolution profiles for carbon dioxide and no methane was observed (therefore propene formation was not due to cracking of isobutane). Therefore propene formation is not accompanied by cracking or combustion of isobutane, instead all carbon atoms from isobutane are used in the production of the olefin. This is supported by previous work which has shown that heteropoly compounds are able to function as dealkylating, alkylating or skeletal isomerisation catalysts [1, 2, 78]. The proposed reaction mechanisms for all observed gas-phase products are:

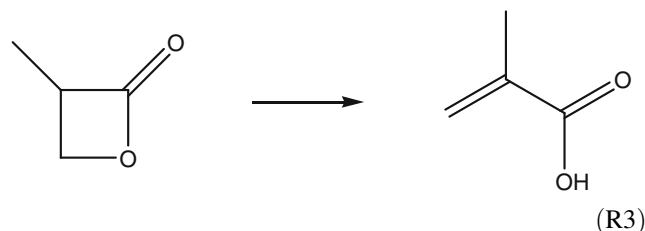
Oxidation and oxidative dehydrogenation of isobutane to form methacrolein



Lactone formation from the oxidation and oxidative dehydrogenation of isobutane



Rearrangement of lactone into methacrylic acid



Formation of acetic acid

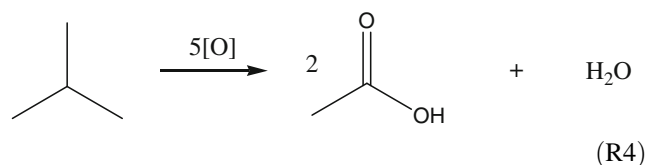
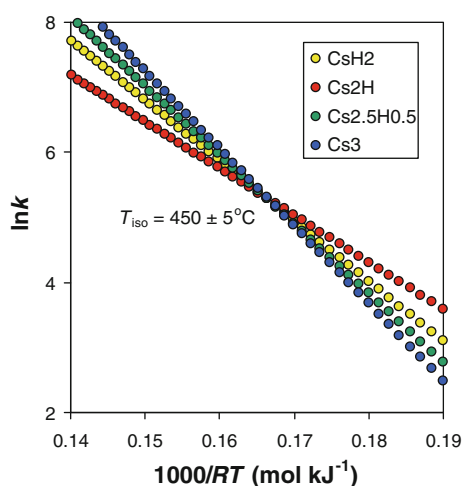
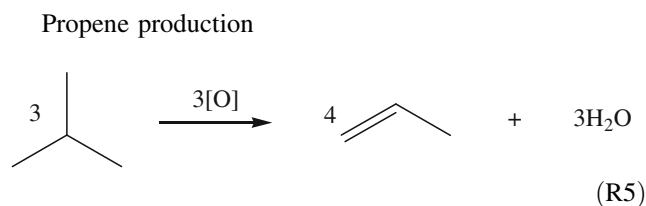


Table 7 Activation energy ranges for Category 2 formations

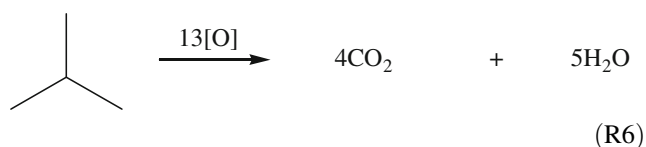
Group 1	MA E_a (kJ mol ⁻¹)	LAC E_a (kJ mol ⁻¹)	AA E_a (kJ mol ⁻¹)	PE E_a (kJ mol ⁻¹)	MAA E_a (kJ mol ⁻¹)
LiH ₂ [PMo ₁₂ O ₄₀]	61–78	122–331	102–123	–	–
Li ₂ H[PMo ₁₂ O ₄₀]	106–242	80–317	72–363	–	–
Li ₃ [PMo ₁₂ O ₄₀]	115	276	–	–	–
NaH ₂ [PMo ₁₂ O ₄₀]	54–123	46–200	–	–	–
Na ₂ H[PMo ₁₂ O ₄₀]	64–141	70–242	–	56–153	–
Na ₃ [PMo ₁₂ O ₄₀]	55–126	–	–	107–123	–
KH ₂ [PMo ₁₂ O ₄₀]	58–278	128–726	–	–	–
K ₂ H[PMo ₁₂ O ₄₀]	54–293	78–234	89–144	–	–
K ₃ [PMo ₁₂ O ₄₀]	85–214	84–257	–	–	–
RbH ₂ [PMo ₁₂ O ₄₀]	70–237	57–317	119–306	–	–
Rb ₂ H[PMo ₁₂ O ₄₀]	–	156–218	–	–	–
Rb ₃ [PMo ₁₂ O ₄₀]	91–146	103–281	–	34–268	–
CsH ₂ [PMo ₁₂ O ₄₀]	73–140	–	–	–	–
Cs ₂ H[PMo ₁₂ O ₄₀]	72–202	–	–	–	–
Cs _{2.5} H _{0.5} [PMo ₁₂ O ₄₀]	–	–	–	–	–
Cs ₃ [PMo ₁₂ O ₄₀]	70–96	–	–	–	–
Group 2					
Mg _{0.5} H ₂ [PMo ₁₂ O ₄₀]	45–122	58–389	–	–	–
MgH[PMo ₁₂ O ₄₀]	58–146	52–274	61–202	–	–
Mg _{1.5} [PMo ₁₂ O ₄₀]	53–114	104–143	–	–	–
Ca _{0.5} H ₂ [PMo ₁₂ O ₄₀]	45–105	70–279	70–181	–	–
CaH[PMo ₁₂ O ₄₀]	50–100	58–116	–	–	–
Ca _{1.5} [PMo ₁₂ O ₄₀]	41–126	73–165	121–210	–	–
Sr _{0.5} H ₂ [PMo ₁₂ O ₄₀]	82–174	69–340	106–225	–	–
SrH[PMo ₁₂ O ₄₀]	65–194	90–161	–	–	–
Sr _{1.5} [PMo ₁₂ O ₄₀]	39–121	88–312	–	–	–
Ba _{0.5} H ₂ [PMo ₁₂ O ₄₀]	81–181	68–76	105–462	–	–
BaH[PMo ₁₂ O ₄₀]	43–180	42–332	83–436	–	167
Ba _{1.5} [PMo ₁₂ O ₄₀]	57–467	68–366	57–253	–	–

**Fig. 8** Arrhenius plots of the four cesium phosphomolybdates. Shown in the figure is the isokinetic temperature; at this temperature the rate of Category 1 methacrolein formation is equivalent**Table 8** Isokinetic parameters obtained from the cesium, calcium and magnesium phosphomolybdates series

Cation	T_{iso} (K)	ω (cm ⁻¹)
Cs ⁺	450 (5)	503 (4)
Mg ²⁺	455 (5)	506 (4)
Ca ²⁺	270 (5)	378 (4)



Complete oxidation of isobutane into carbon dioxide and water



All reactions occur concurrently, with the exception of (R3) which is thought to occur consecutively as a rearrangement from lactone. In these reaction steps [O] represents oxygen atoms contained in the phosphomolybdate anion and are known as lattice or framework oxygens. For example, complete oxidation of isobutane requires 13[O]. These reactions occur through a Mars-van Krevelen mechanism in which lattice oxygens are used for oxidation and are then replaced by molecular oxygen if present in the reactant feed stream [25, 45, 70, 72, 79–85]. Oxygen has not been included in the reactant feed stream for this work as it complicates both the molecular flow conditions and resolution of peak intensities, therefore the lattice oxygens are not replenished. This should result in a reduction of the catalyst over time, yet the low reactant feed stream flux of 10^{15} molecules per second (of which half is isobutane and half is argon) results in a very small proportion of oxygen atoms being removed from the structure during experiments and hence this effect is insignificant. Additionally, contact times in the Knudsen cell reactor are relatively short. Each of the proposed reaction steps involve water evolution, which is observed for isobutane conversion over phosphomolybdic acid and its derivatives.

3.6 Factors Influencing Activity

3.6.1 Pseudoliquid Phase, Surface and Bulk Catalysis

Heteropoly compounds have a unique ability to absorb molecules into their bulk [86]. This phenomenon is associated with rapid migration of reactant and products species through the bulk in a manner which resembles liquid diffusion, and hence the phase this creates is termed “pseudoliquid”. Another characteristic of heteropoly compounds is their ability to undergo reactions inside the catalyst bulk as well as on the surface [17, 87–90]. The bulk processes are categorised into two distinct variants, labeled Bulk-types (I) and (II). Bulk-type (I) is concerned with reactants migrating deep within the solid to undergo reactions, with the subsequent products migrating to the surface and desorbing. This type of reaction is due to pseudoliquid behavior [69]. Bulk-type (II) processes consist of reactants undergoing reaction on the surface of the catalyst where the reaction is controlled by the rapid

migration of redox carriers (electrons and protons) throughout the catalyst bulk. Because reaction molecules do not migrate through the solid, Bulk-type (II) is not related to pseudoliquid behavior. Nevertheless both Bulk-types occur in a three dimensional reaction field [91], therefore surface area of the catalyst does not impact on reaction rates [17].

Category 1 methacrolein formation occurs only with isobutane in the feed stream and the distributions are empirically consistent with a Langmuir adsorption isotherm model. This suggests that reactants are adsorbing as monolayers on the surface rather than penetrating the bulk [92] and hence Category 1 methacrolein forms via reaction on the surface. Therefore the Category 1 methacrolein formation occurs either as a pure surface-type reaction with no involvement from the bulk of the phosphomolybdates, or a Bulk-type (II) mechanism operates whereby isobutane adsorption and methacrolein formation are restricted to the surface but electron and proton migration through the bulk facilitates the reaction. Previous work on similar reactions for the oxidative dehydrogenation of isobutyraldehyde and isobutyric acid to yield methacrolein and methacrylic acid respectively, have suggested that products are formed via a Bulk-type (II) mechanism [34, 69, 93]. Surface area has been shown to increase with respect to cesium content in phosphomolybdic acid derivatives [6, 34, 69], although this is not reflected in the Arrhenius parameters given in Table 6. It is therefore inferred that a simple surface-type reaction is not associated with Category 1 methacrolein formation over the phosphomolybdates and therefore a Bulk-type (II) process predominates.

Category 2 methacrolein, lactone, acetone, propene and methacrylic acid form with or without gas-phase isobutane and production occurs in bell-shaped distributions typically observed with desorption and reactant coverage proceeds past monolayer extent. Therefore Category 2 product formation is consistent with isobutane penetrating deep inside the bulk of the phosphomolybdates, undergoing reaction and creating products which later desorb from the surface. These considerations suggest the establishment of a pseudoliquid phase and Bulk-type (I) processes for the Category 2 reaction mechanisms. The profiles that are associated with the Category 2 distributions may be representative of successive reductions of the phosphomolybdate anion. For example, the lowest temperature peak corresponds to the reduction of a phosphomolybdate anion or region of anions. Successive product formations occur from progressively more reduced phosphomolybdates anions. In this way each bell-shaped distribution coincides with reaction of isobutane with phosphomolybdate anions of a particular oxidation state and environment. The formation of different products via parallel reactions at neighboring active sites would also affect the reduction of

the heteropolyanion, either locally or as a whole. Hence the creation of a particular product may directly impact on another in a complicated manner. The cesium derivatives seem to be unique in that the only product observed is methacrolein, though this occurs via both Category 1 and 2 processes. Perhaps cesium addition prevents isobutane migration deep into the bulk of the solid whereby higher oxidation products are unable to form. Work conducted by Okuhara et al. supports this conclusion [94].

3.6.2 Investigation into Correlations

Previous work has shown that catalyst activity varies markedly depending upon counter cation selection and there is no clear relationship between the amount of cation and activity [87]. Several attempts have been made to link the activity of a catalyst with the physical and chemical properties of the associated cations and these include: ionic radius [35], ionic potential [34], electronegativity [95–101], enthalpy of oxide formation [99, 102, 103], electronic polarisability [95, 104, 105] and optical basicity [106–113]. All of these parameters are listed in Table 9. With the exception of $\Delta_f H^\theta$ for cesium oxide and magnesium oxide, the parameters progressively increase or decrease down each of Groups 1 and 2. Provided the activity and selectivity properties of the solids increased or decreased down a particular Group, a relationship might be established with any of the values. The Category 1 and 2 distributions presented in this thesis, and their corresponding kinetic parameters, show no such simple trend or obvious volcano plot. For example, the reasons why cesium, magnesium and calcium salts display Category 1 methacrolein formation or why some phosphomolybdates form acetic acid, cannot be readily concluded from the values in Table 9 (whether viewed in isolation or in various multiplicative or divisionary combinations). It may be that one or more of these parameters impacts on the selectivity and activity of the phosphomolybdates, though the contribution would be a factor only, and the identification of other properties is required to elucidate a meaningful association.

Selective oxidation of isobutane conducted by Paul et al. [44] over a similar catalyst to those used in this work, $(\text{Cs}^+/\text{NH}_4^+/\text{H}^+)_4[\text{PMo}_{11}\text{VO}_{40}]$, determined the reduction of the structure exhibited an activation energy of 90.4 kJ mol^{-1} . This is comparable to the activation energies measured for Category 1 methacrolein production over the cesium phosphomolybdates (Table 6). This further supports the hypothesis that Category 1 methacrolein forms via a Bulk-type (II) mechanism. In light of this, and considering that the oxidation of isobutane necessitates reduction of the phosphomolybdates structure, it may be that all rates of all product formation are determined by the reduction

capabilities of the solids. Furthermore, the large activation barriers experienced by some of the higher temperature profiles from the Category 2 distributions may be reflective of creating products from already highly reduced active sites.

4 Summary and Conclusions

Phosphomolybdates were synthesized from cationic exchange of phosphomolybdic acid with cations of Groups 1 and 2 of the periodic table. The Group 1 cations were Li^+ , Na^+ , K^+ , Rb^+ and Cs^+ and the Group 2 cations were Mg^{2+} , Ca^{2+} , Sr^{2+} and Ba^{2+} . Three compounds of differing cationic ratios were synthesized from each cation, except for the cesium salts, of which four were made.

XRD data from analysis of pure phosphomolybdic acid showed the presence of a triclinic phase exclusively. Group 1 phosphomolybdates exhibit a range of structural phases. At low cationic volumes the triclinic structure is present, while at high volumes the body centered cubic phase predominates. The body centered cubic phase forms once the cationic volume exceeds about $9\text{--}11 \text{ \AA}^3$. Group 2 compounds possess a triclinic phase, however an increase in the cationic volume is associated with a decreasing contribution of the (110) plane to the structure and an introduction of some amorphous character. This occurs once cationic volume is greater than about $5\text{--}6 \text{ \AA}^3$.

Two distinct types of reactions were identified and classified as either Category 1 or Category 2. Product formation for Category 1 distributions increases with increasing temperature, in a manner consistent with an exponential distribution and only occurs whilst gas-phase isobutane is present. Category 2 profiles consist of several peaks (although sometimes a single peak is observed), usually overlapping and only resolvable into individual peaks by extensive modeling with Gaussian curves; this type of distribution is observed with or without gas-phase isobutane.

Products observed from the oxidation of isobutane were methacrolein, lactone (3-methyl-2-oxetanone), acetic acid, propene, methacrylic acid, carbon dioxide and water. The partial and total substitution of protons with Group 1 and 2 cations resulted in a large reduction of complete oxidation products, i.e. carbon dioxide and water; these are difficult to quantify and are of little interest, so they were excluded from the modeling procedure. Methacrolein formation occurs via both Category 1 and Category 2 processes, whilst lactone, acetic acid, propene, and methacrylic acid are exclusively Category 2 reactions. Propene was only observed with the Group 1 compounds $\text{Na}_2\text{H}[\text{PMo}_{12}\text{O}_{40}]$, $\text{Na}_3[\text{PMo}_{12}\text{O}_{40}]$ and $\text{Rb}_3[\text{PMo}_{12}\text{O}_{40}]$, whilst methacrylic acid production was restricted to a

Table 9 Values of ionic radius (r_i), ionic potential (p_i), electronegativity (χ), enthalpy of oxide formation ($\Delta_f H^\theta$), electronic polarisability (α) and optical basicity (Λ)

Cation	r_i (Å) [35]	p_i (charge/ r_i)*	χ [95]	$\Delta_f H^\theta$ (kJ mol ⁻¹) [102]	α (10 ⁻²⁴ cm ³) [95]	Λ
Li ⁺	0.76	1.84	0.98	-598	0.029	0.81
Na ⁺	1.02	4.45	0.93	-414	0.179	1.10
K ⁺	1.38	11.0	0.82	-363	0.83	1.30
Rb ⁺	1.52	14.7	0.82	-339	1.40	1.45
Cs ⁺	1.67	19.5	0.79	-346	2.42	1.55
Mg ²⁺	0.72	2.78	1.31	-602	0.094	0.61
Ca ²⁺	1.00	2.00	1.00	-635	0.47	1.00
Sr ²⁺	1.18	1.69	0.95	-592	0.86	1.05
Ba ²⁺	1.35	1.48	0.89	-554	1.55	1.35

* Here ionic potential is defined as the ratio of cation charge to ionic radius. All radii refer to cation in six coordination state

single catalyst, BaH[PMo₁₂O₄₀]. The isobutane oxidation products form in various quantities depending on cation selection. Methacrolein was the only product observed over the cesium phosphomolybdates, showing that cesium addition yields highly selective substrates.

Methacrolein production occurs without evidence of isobutene-like intermediary species and most likely forms via a one-step oxidation of isobutane. Likewise, lactone, acetic acid, propene and carbon dioxide occur in parallel reactions. However methacrylic acid, observed over BaH[PMo₁₂O₄₀], mirrors a lactone formation profile over the same catalyst. This intimates that lactone is a precursor to methacrylic acid formation. Nguyen et al. have shown that the lactone rearranges into methacrylic acid via catalysis by water and acid [38]. It is proposed that lactone rearranges to methacrylic acid under normal reaction conditions of high pressures but is instead isolated in this work due to the molecular flow regime. Therefore all reactions are thought to occur in parallel, with the exception of methacrylic acid, which is created from lactone rearrangement.

All phosphomolybdates showed excellent stability and consistent kinetic results, except for the parent acid which experienced cumulative structural degradation over successive experiments. Arrhenius parameters have been calculated for the Category 1 and 2 distributions. The lowest calculated activation for Category 1 methacrolein formation is 34.7 ± 1.3 kJ mol⁻¹ over the LiH₂[PMo₁₂O₄₀] compound, while the highest recorded is 149 ± 4 kJ mol⁻¹ for the fourth experiment over H₃[PMo₁₂O₄₀]. The Category 2 kinetic parameters were extensive and ranged from 34.3 ± 0.4 kJ mol⁻¹ (for the third propene profile over Rb₃[PMo₁₂O₄₀]) to 726 ± 172 kJ mol⁻¹ (occurring with the fourth lactone peak over KH₂[PMo₁₂O₄₀]).

Salts of cesium, magnesium and calcium exhibit a phenomenon known as the “isokinetic point”. This refers to the existence of a temperature at which all compounds containing a particular cation have the same rate of Category 1 methacrolein formation. For cesium, magnesium

and calcium phosphomolybdates the respective isokinetic temperatures are 450 ± 5 , 455 ± 5 and 270 ± 5 °C and the transition state frequencies are 503 ± 4 , 506 ± 4 , 378 ± 4 cm⁻¹. The transition state frequencies do not correspond to methacrolein vibrations, as calculated using Gaussian 03 software, hence the transition state geometries are likely to be significantly different than the fully formed methacrolein. However, the similar methacrolein transition state frequencies for the cesium and magnesium compounds indicate that methacrolein forms in a comparable manner over these phosphomolybdates.

Several theories have been proposed by previous researchers to account for activity: ionic radius, ionic potential, electronegativity, enthalpy of oxide formation, electronic polarisability, and optical basicity. However none of these adequately describes the activity observed and no clear linear or volcano relationships could be ascertained between the Arrhenius parameters and properties of the cations. Category 1 methacrolein formation is proposed to form via a Bulk-type (II) mechanism, where the reaction occurs on the surface, but this is accompanied by rapid migration of electrons and protons deep into the bulk of the solid. Category 2 product formations of methacrolein, lactone, acetic acid and propene are Bulk-type (I) reactions, which also involve charge transfer; these occur when the actual reactant penetrates deep into the bulk of the solid to form products, which migrate to the surface and desorb. Therefore, electronic properties of the substrates likely determine reaction kinetics, rather than geometric properties. Indeed previously work by Paul et al. indicates that reduction of the substrate may be rate determining [44].

References

1. Okuhara T, Mizuno N, Misono M (1996) Adv Catal 41:113–252
2. Misono M (2001) Chem Commun 13:1141–1152

3. Furuta M, Sakata K, Misono M, Yoneda Y (1979) *Chem Lett* 8:31–34
4. Pope MT (1983) *Heteropoly and isopoly oxometalates*. Springer-Verlag, Berlin
5. Moffat JB (2001) *Metal-oxygen clusters*. Kluwer, New York
6. Langpape M, Millet JMM, Ozkan US, Boudeulle M (1999) *J Catal* 181:80–90
7. Etienne E, Cavani F, Mezzogori R, Trifirò F, Calestani G, Gengembre L, Guelton M (2003) *Appl Catal A Gen* 256:275–290
8. McGarvey GB (1988) *J Colloid Interf Sci* 125:51–60
9. McMonagle JB, Moffat JB (1984) *J Colloid Interf Sci* 101:479–488
10. Mizuno N, Suh DJ, Han W, Kudo T (1996) *J Mol Catal A Chem* 114:309–317
11. Rocchiccioli-Deltcheff C, Aouissi A, Bettahar MM, Launay S, Fournier M (1996) *J Catal* 164:16–27
12. Silviani E, Burns RC (2004) *J Mol Catal A Chem* 219:327–342
13. Taylor DB, McMonagle JB, Moffat JB (1985) *J Colloid Interf Sci* 108:278–284
14. Wienold J, Timpe O, Ressler T (2003) *Chem Eur J* 9:6007–6017
15. Black JB, Clayden NJ, Gai PL, Scott JD, Serwicka EM, Goodenough JB (1987) *J Catal* 106:1–15
16. McGarvey GB, Moffat JB (1992) *Catal Lett* 16:173–180
17. Mizuno N, Watanabe T, Mori H, Misono M (1990) *J Catal* 123:157–163
18. Okuhara T, Hashimoto T, Misono M, Yoneda Y (1983) *Chem Lett* 12:573–576
19. WP Coverage of Methyl Methacrylate (MMA). SRI Consulting (2010). <http://www.sriconsulting.com/WP/Public/Reports/mma/>
20. Deusser LM, Petzoldt JC, Gaube JW, Hibst H (1998) *Ind Eng Chem Res* 37:3230–3236
21. Nagai K (2001) *Appl Catal A Gen* 221:367–377
22. Kendell SM, Alston A-S, Ballam NJ, Brown TC, Burns RC (2011) *Catal Lett* 141:374–390
23. Kendell SM, Brown TC (2010) *React Kinet Mech Catal* 99:251–268
24. Kendell SM, Brown TC, Burns RC (2008) *Catal Today* 131:526–532
25. Mars P, van Krevelen DW (1954) *Chem Eng Sci (Spec Suppl)* 3:41–59
26. Le Minh C, Brown TC (2006) *Appl Catal A Gen* 310:145–154
27. Chang TH (1995) *J Chem Soc Faraday Trans* 91:375–379
28. Fournier M, Feumi-Jantou C, Rabia C, Hervé G, Launay S (1992) *J Mater Chem* 2:971–978
29. West SF, Audrieth LF (1955) *J Phys Chem* 59:1069–1072
30. Silviani E (2003) PhD thesis, University of Newcastle, Australia
31. Eguchi K, Toyozawa Y, Furuta K, Yamazoe N, Seiyama T (1981) *Chem Lett* 1253–1256
32. Eguchi K, Yamazoe N, Seiyama T (1981) *Nippon Kagaku Kaishi* 336
33. Christian JB, Whittingham MS (2008) *J Solid State Chem* 181:1782–1791
34. Hu J, Burns RC (2000) *J Catal* 195:360–375
35. Shannon RD (1976) *Acta Crystallogr A* 32:751
36. Cavani F (1998) *Catal Today* 41:73–86
37. Jurgensen A, Moffat JB (1995) *Catal Lett* 34:237–244
38. Nguyen NH, Kendell S, Le Minh C, Brown T (2010) *Catal Lett* 136:28–34
39. Hunger B, Klepel O, Kirschhock C, Heuchel M, Toufar H, Fuess H (1999) *Langmuir* 15:5937–5941
40. Qian EW, Horio T, Sutrisna IP (2009) *Energy Fuels* 23:1583–1590
41. Beta IA, Hunger B, Böhlig H (2001) *J Therm Anal Calorim* 64:1191–1199
42. Niwa M, Katada N (1997) *Catal Surv Jpn* 1:215–226
43. Kendell S, Alston A, Brown T (2009) *Chem Prod Process Model* 4:5
44. Paul S, LeCourtis V, Vanhove D (1997) *Ind Eng Chem Res* 36:3391–3399
45. Mizuno N, Yahiro H (1998) *J Phys Chem B* 102:437–443
46. Jalowiecki-Duhamel L, Monnier A, Barbaux Y, Hecquet G (1996) *Catal Today* 32:237–241
47. Liu-Cai FX, Pham C, Bey F, Herve G (2002) *React Kinet Catal Lett* 75:305–314
48. Li W, Ueda W (1997) *Catal Lett* 46:261–265
49. Schindler GP, Ui T, Nagai K (2001) *Appl Catal A Gen* 206:183–195
50. Guan J, Jia M, Jing S, Wang Z, Xing L, Xu H, Kan Q (2006) *Catal Lett* 108:125–129
51. Sun Y, Brown TC (2000) *J Catal* 194:301–308
52. Savitzky A, Golay M (1964) *Anal Chem* 36:1627–1639
53. Bligaard T, Honkala K, Logadottir A, Norskov JK (2003) *J Phys Chem B* 107:9325–9331
54. Conner WC Jr (1983) *J Catal* 84:273–274
55. Galwey AK, Mortimer M (2006) *Int J Chem Kinet* 38:464–473
56. Karpinski Z, Larsson R (1997) *J Catal* 168:532–537
57. Larsson R (1989) *J Mol Catal* 55:70–83
58. Larsson R (1998) *Appl Catal A Gen* 167:N12–N13
59. Linert W (1994) *Chem Soc Rev* 23:429–438
60. Linert W, Jameson RF (1989) *Chem Soc Rev* 18:477–505
61. Patterson WR, Rooney JJ (1994) *J Catal* 146:310–312
62. Rooney JJ (1998) *Catal Lett* 50:15
63. Rooney JJ (1998) *Appl Catal A Gen* 166:N3
64. Galwey A (1983) *J Catal* 84:270–272
65. Schwab GM (1983) *J Catal* 84:1–7
66. Rooney JJ (1995) *J Mol Catal* 96:L1–L3
67. Paul JS, Jacobs PA, Weiss PAW, Maier WF (2004) *Appl Catal A Gen* 265:185–193
68. Shishido T, Inoue A, Konishi T, Matsuura I, Takehira K (2000) *Catal Lett* 68:215–221
69. Mizuno N, Tateishi M, Iwamoto M (1996) *J Catal* 163:87–94
70. Busca G, Cavani F, Etienne E, Finocchio E, Galli A, Selleri G, Trifiro F (1996) *J Mol Catal A Chem* 114:343–359
71. Bentrup U, Bruckner A, Kant M, Kolff S, Dingerdissen U, Jansen S, Maschmeyer D, Siegert H, Zanthoff W (2006) *Erdöl Erdgas Kohle* 122:OG145–OG148
72. Cavani F, Mezzogori R, Pigamo A, Trifiro F, Etienne E (2001) *Catal Today* 71:97–110
73. Cavani F, Etienne E, Favaro M, Galli A, Trifiro F, Hecquet G (1995) *Catal Lett* 32:215–226
74. Konishi Y, Sakata K, Misono M, Yoneda Y (1982) *J Catal* 77:169–179
75. Misono M, Komaya T, Sekiguchi H, Yoneda Y (1982) *Chem Lett* 53–56
76. Marosi L, Cox G, Tenten A, Hibst H (2000) *J Catal* 194:140–145
77. Marosi L, Cox G, Tenten A, Hibst H (2000) *Catal Lett* 67:193–196
78. Kozhevnikov IV (1993) *Russ Chem Rev* 62:473–491
79. Schindler GP, Knapp C, Ui T, Nagai K (2003) *Top Catal* 22:117–121
80. Andersson SLT (1994) *Appl Catal A Gen* 112:209–218
81. Creaser D, Andersson B (1996) *Appl Catal A Gen* 141:131–152
82. Late L, Blekkan EA (2002) *J Nat Gas Chem* 11:33–42
83. Doornkamp C, Ponc V (2000) *J Mol Catal A Chem* 162:19–32
84. Vannice MA (2007) *Catal Today* 123:18–22
85. Brazdil JF, Suresh DD, Grasselli RK (1980) *J Catal* 66:347–367
86. Misono M (2000) *Comptes Rendus de l'Academie des Sciences Series IIC Chemistry Sciences* 3:471–475
87. Komaya T, Misono M (1983) *Chem Lett* 12:1177–1180
88. Misono M (1987) *Mater Chem Phys* 17:103–120

89. Okuhara T, Kasai A, Hayakawa N, Misono M, Yoneda Y (1981) *Chem Lett* 391–394
90. Okuhara T, Kasai A, Hayakawa N, Yoneda Y, Misono M (1983) *J Catal* 83:121–130
91. Misono M (1992) *Catal Lett* 12:63–72
92. Atkins PW (1994) *Physical chemistry*, 5th edn. Oxford University Press, Oxford
93. Misono M (1987) *Catal Rev Sci Eng* 29:269–321
94. Okuhara T, Arai T, Ichiki T, Lee KY, Misono M (1989) *J Mol Catal* 55:293–301
95. Lide DR (2002–2003) *CRC handbook of chemistry and physics*, 83rd edn. CRC Press, Boca Raton
96. Allen LC (1989) *J Am Chem Soc* 111:9003–9014
97. Allred AL (1961) *J Inorg Nucl Chem* 17:215–221
98. Pauling L (1960) *The nature of the chemical bond*, 3rd edn. Cornell University Press, Ithaca
99. Ai M (1982) *Appl Catal* 4:245–256
100. Ai M (1981) *J Catal* 71:88–98
101. Akimoto M, Tsuchida Y, Echigoya E (1980) *Chem Lett* 1205–1208
102. Aylward G, Findlay T (1998) *SI chemical data*, 4th edn. Jacaranda Wiley Limited, Singapore
103. Stytsenko VD, Lee WH, Lee JW (2001) *Kinet Catal* 42:212–216
104. Pauling L (1927) *Proc R Soc Lond Ser A* 114:181–211
105. Idriss H, Seebauer EG (2000) *Catal Lett* 66:139–145
106. Dimitrov V, Komatsu T (2002) *J Solid State Chem* 163:100–112
107. Leboutteiller A, Courtine P (1998) *J Solid State Chem* 137:94–103
108. Moriceau P, Leboutteiller A, Bordes E, Courtine P (1999) *Phys Chem Chem Phys* 1:5735–5744
109. Moriceau P, Taouk B, Bordes E, Courtine P (2000) *Catal Today* 61:197–201
110. Zhao X, Wang X, Lin H, Wang Z (2007) *Physica B* 392:132–136
111. Duffy JA, Ingram MD (1971) *J Am Chem Soc* 93:6448–6454
112. Duffy JA, Ingram MD (1976) *J Non-Cryst Solids* 21:373–410
113. Fierro JLG (2006) *Metal oxides chemistry and applications*. Taylor and Francis, Boca Raton